

# Drive-Through Quantum Gate: Non-Stop Entangling a Mobile Ion Qubit with a Stationary One

Ting Hsu<sup>1,2,5</sup>, Wen-Han Png<sup>3</sup>, Kuan-Ting Lin<sup>5</sup>, Ming-Shien Chang<sup>4</sup> and Guin-Dar Lin<sup>1,2,5</sup>

<sup>1</sup>*Department of Physics and Center for Quantum Science and Engineering,  
National Taiwan University, Taipei 10617, Taiwan*

<sup>2</sup>*Physics Division, National Center for Theoretical Sciences, Taipei 10617, Taiwan*

<sup>3</sup>*Centre for Quantum Technologies, National University of Singapore, 3 Science Drive 2, Singapore 117543*

<sup>4</sup>*Institute of Atomic and Molecular Sciences, Academia Sinica, Taipei 10617, Taiwan*

<sup>5</sup>*Trapped-Ion Quantum Computing Laboratory, Hon Hai Research Institute, Foxconn, Taipei 11492, Taiwan*

Towards the scalable realization of a quantum computer, a quantum charge-coupled device (QCCD) based on ion shuttling has been considered a promising approach. However, the processes of detaching an ion from an array, reintegrating it, and driving non-uniform motion introduce severe heating, requiring significant time and laser power for re-cooling and stabilization. To mitigate these challenges, we propose a novel entangling scheme between a stationary ion qubit and a continuously transported mobile ion, which remains in uniform motion and minimizes motional heating. We theoretically demonstrate a gate error on the order of 0.01%, within reach of current technology. This approach enables resource-efficient quantum operations and facilitates long-distance entanglement distribution, where stationary trapped-ion arrays serve as memory units and mobile ions act as communication qubits passing beside them. Our results pave the way for an alternative trapped-ion architecture beyond the QCCD paradigm.

**Introduction.** Trapped ions are among the leading platforms for quantum information processing [1, 2], offering unparalleled coherence times [3], high-fidelity gate operations [4–6], and straightforward qubit initialization and readout [3]. The inherent long-range Coulomb interaction enables all-to-all connectivity in principle, allowing for scalable entanglement in linear ion chains or two-dimensional ion lattices [7–9]. However, beyond hundreds of ions, the increasing number of vibrational modes complicates mode addressing, laser control suffers from cross-talk and challenges in maintaining individual ion addressing, and the interaction strength between distant ions weakens significantly [10–12]. These factors present fundamental challenges to scaling large trapped-ion quantum processors. As system size continues to increase, preserving these advantages while maintaining efficient and controllable connectivity becomes a central challenge for trapped-ion architectures.

In response to these challenges, modular ion-trap architectures have been proposed, leveraging either photonic interconnects [13–15] or ion shuttling [16, 17]. While photonic links enable entanglement over long distances, atom-photon interactions are inherently weak and probabilistic, resulting in poor photon collection efficiency and low success rates [18]. The alternative approach, shuttling-based architectures such as the quantum charge-coupled device (QCCD), allows deterministic entangling operations by transporting qubits into proximity through a sequence of transport steps – linear motion, merging, splitting, and swapping [19, 20]. However, as quantum circuits grow in complexity, the number of transport operations required in a QCCD increases rapidly, leading to cumulative motional heating and decoherence [21]. While laser and sympathetic cooling can mitigate motional heating, these procedures significantly extend operational time and increase laser

power consumption [19]. These considerations indicate that transport-related overhead can become a limiting factor in modular trapped-ion architectures, particularly as the number of required transport operations increases.

To address these limitations, we propose a novel entangling scheme with minimal transport overhead. As illustrated in Fig. 1a, a moving ion, serving as a communication qubit, passes by a stationary ion that acts as a memory qubit, while maintaining uniform motion throughout the interaction. By incorporating the time-dependent Coulomb interaction into the gate design, we theoretically demonstrate an entangling gate with errors on the order of  $10^{-4}$ , achieved without requiring additional cooling or stopping of the mobile qubit. The same moving ion can subsequently interact with multiple stationary qubits in a sequential manner, effectively functioning as a mobile quantum bus for long-range entanglement generation. We refer to this scheme as the drive-through gate (DTG).

Conventional trapped-ion architectures rely on entangling operations performed at well-defined stopping points, where transported ions are merged into stationary chains and subsequently re-separated. In contrast, the DTG scheme removes the requirement that transport qubits must be brought to rest for gate execution. Entanglement is instead generated during continuous motion, with qubits remaining either stationary or in uniform transport throughout the operation. While quantum gates between co-moving ions have been demonstrated previously [22, 23], such schemes rely on synchronized motion and do not address the scaling overhead associated with repeated stopping, cooling, and reconfiguration steps. By shifting the entangling interaction from discrete stopping points to continuous transport, the DTG scheme defines a distinct operational paradigm for modular distributed trapped-ion quantum computing,

enabling interactions between spatially separated memory units with reduced transport-induced overhead.

## Results

**Setup.** To illustrate the DTG scheme, we consider a two-ion system as shown in Fig. 1a. Ion 1 is confined by a stationary harmonic trap whose center is fixed at  $Q_1 = (0, 0, 0)$  while ion 2 is captured by a moving harmonic trap whose center follows a prescribed trajectory  $Q_2(t) = (d, vt, 0)$ . In the presence of the Coulomb interaction, the equilibrium position of each ion is shifted relative to the center of its trapping potential. The actual position of the  $i$ -th ion can therefore be written as  $\mathbf{q}_i(t) = \mathbf{q}_i^{(0)}(t) + \boldsymbol{\xi}_i(t)$ , where  $\mathbf{q}_i^{(0)}(t)$  denotes the instantaneous equilibrium position and  $\boldsymbol{\xi}_i(t)$  describes small motional oscillation around it. In the adiabatic shuttling regime considered here, these oscillations remain small compared to the inter-ion separation, allowing the transverse motion to be treated independently from the in-plane transport.

In the following, we focus on the transverse ( $z$ ) motional modes for gate implementation. This choice is motivated by experimental considerations: residual acceleration arising from electrode noise primarily affects in-plane transport, and laser coupling to in-plane modes is more susceptible to Doppler shifts during shuttling. By operating along the transverse direction, these effects are naturally suppressed, allowing the gate dynamics to be analyzed within a more controlled regime. This separation enables a time-dependent normal-mode description that remains well-defined throughout the transport process.

**Dynamical motional normal modes.** In the adiabatic shuttling regime, the motional oscillations  $\boldsymbol{\xi}_i(t)$  around the equilibrium positions satisfy  $|\boldsymbol{\xi}_i(t)| \ll R(t)$ , where  $R(t) = |\mathbf{q}_1^{(0)}(t) - \mathbf{q}_2^{(0)}(t)|$  denotes the time-dependent separation between the instantaneous equilibrium positions of the two ions. Under this condition, the Coulomb interaction can be expanded to second order in the transverse motion, leading to an effective quadratic Hamiltonian  $\hat{H}_0(t) = \sum_i \frac{\hat{p}_i^2}{2m} + \frac{1}{2} \sum_{i,j=1}^2 G_{ij} \hat{z}_i \hat{z}_j$ , where  $\hat{z}_i$  denotes the transverse position operator of the  $i$ th ion measured from its instantaneous equilibrium position  $\mathbf{q}_i^{(0)}(t)$ , and  $G_{ij} = m\omega_z^2 \delta_{ij} - \frac{K}{R^3(t)} (-1)^{i+j}$ , with  $K = \frac{e^2}{4\pi\epsilon_0}$ .

Following the dynamical normal-mode formalism of Ref. [24], because the two ions are of the same species and experience identical local confinement, the transverse motion can be described in terms of the dynamical normal modes despite the time-dependent Coulomb coupling. The system admits a center-of-mass mode and a zigzag mode with time-dependent frequencies

$$\Omega_1(t) = \omega_z, \quad (1)$$

$$\Omega_2(t) = \sqrt{\omega_z^2 - \frac{2K}{mR^3(t)}}. \quad (2)$$

In this basis, the Hamiltonian becomes diagonal,

$$\hat{H}_0(t) = \frac{1}{2} \sum_{n=1}^2 \left[ \frac{\hat{P}_n^2}{m} + m\Omega_n^2(t) \hat{Z}_n^2 \right], \quad (3)$$

where  $\hat{Z}_n$  and  $\hat{P}_n$  are the canonical position and momentum operators associated with the  $n$ th dynamical normal mode.

**Gate design.** The drive-through gate is implemented using a state-dependent force that couples the internal qubit states to the transverse motional degrees of freedom. When the moving ion enters the operation region, laser beams are simultaneously applied to both ions to generate a spin-dependent displacement along the transverse ( $z$ ) direction.

In the Lamb–Dicke regime, where the motional scales are small compared to the optical wavelength, the laser-ion interaction can be expressed, in the dynamical normal-mode basis, as  $\hat{H}_1(t) = f(t) \sum_{j,n=1}^2 b_j^n \hat{Z}_n \hat{\sigma}_j^z$ . Here,  $\hat{\sigma}_j^z$  denotes the Pauli operator of the  $j$ th ion,  $\hat{Z}_n$  is the position operator of the  $n$ th dynamical normal mode, and  $b_j^n$  is the corresponding mode participation coefficient. The time-dependent force amplitude is given by  $f(t) = -\hbar k \chi(t) \sin \mu t$  [25, 26], where  $\chi(t)$  is the effective Rabi frequency envelope,  $k$  is the effective wavenumber of the laser field, and  $\mu$  is the detuning relative to the qubit transition. The laser is applied only when the moving ion traverses a finite operation region of width  $w$  along its trajectory, such that  $\chi(t) = 0$  outside this interval. The total Hamiltonian of the system is therefore  $\hat{H}(t) = \hat{H}_0(t) + \hat{H}_1(t)$ , which forms the starting point for the derivation of the drive-through entangling gate.

DTG differs from conventional geometric phase gates in that the motional mode frequencies  $\Omega_n(t)$  vary in time during the interaction. Nevertheless, the underlying mechanism is the same: a state-dependent force induces conditional displacements in phase space, and a closed-loop trajectory yields a qubit-state-dependent geometric phase.

To make this explicit, we perform a unitary transformation with the unitary operator

$$\hat{U}_D = \exp \left\{ \frac{i}{\hbar} \sum_{j,n=1}^2 \left[ m\dot{u}_n(t) \hat{Z}_n - u_n(t) \hat{P}_n \right] b_j^n \hat{\sigma}_j^z \right\} \quad (4)$$

where  $u_n(t)$  satisfies the classical equation of motion of a driven oscillator with time-dependent frequency,

$$\ddot{u}_n(t) + \Omega_n^2(t) u_n(t) = \frac{f(t)}{m}, \quad (5)$$

together with initial conditions  $u_n(t_0) = 0$  and  $\dot{u}_n(t_0) = 0$  so that  $\hat{U}_D(t_0) = \hat{I}$ . Under this transformation, the Hamiltonian  $\hat{H}(t)$  is mapped into  $\tilde{H}(t) = \hat{U}_D \hat{H}(t) \hat{U}_D^\dagger - i\hbar \hat{U}_D \frac{\partial \hat{U}_D^\dagger}{\partial t} = \hat{H}_0(t) + \hat{\theta}(t)$ , where  $\hat{\theta}$  contains only spin

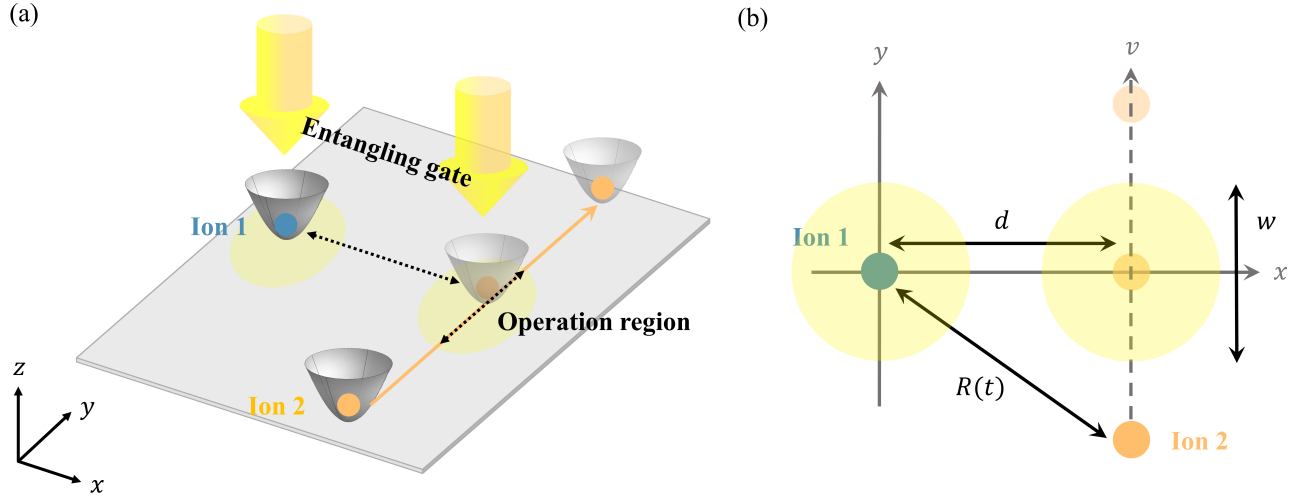


Figure 1. **Drive-through gate scheme.** (a) Schematic representation of the drive-through gate scheme for a two-ion system. The local trap of ion 1 is stationary while the local trap of ion 2 is shuttled along a straight path in the  $x$ - $y$  plane. The entangling operation is performed as ion 2 moves through the operation region. (b) Ion 2 undergoes uniform motion with speed  $v$ , leading to a time-dependent Coulomb interaction characterized by  $R(t)$ , the inter-ion separation. The laser beam, with a spatial width  $w$ , defines the operation region where the drive-through gate is performed.

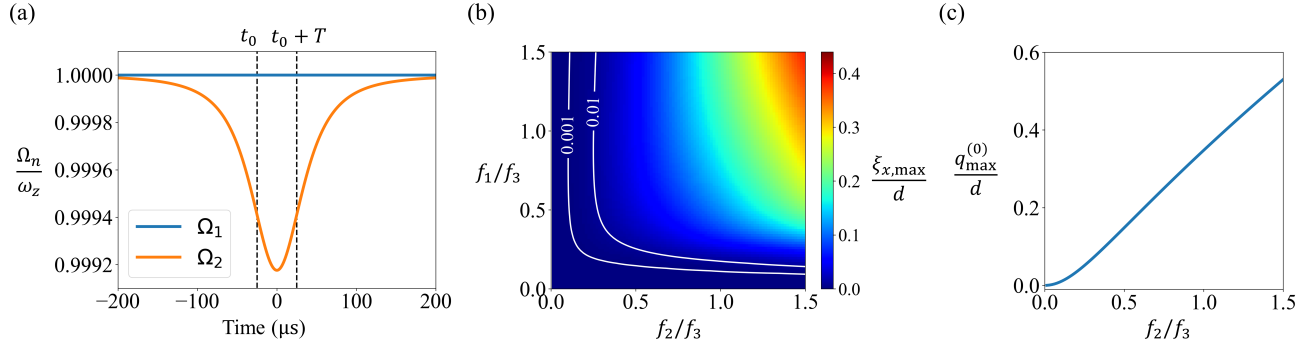


Figure 2. **Dynamical normal modes and parameter regimes for the DTG scheme.** (a) The dynamical normal mode frequencies. The blue and orange curves correspond to the center-of-mass mode  $\Omega_1$  and zigzag mode  $\Omega_2$ , respectively. The trapping frequency is  $\omega_{x,y} = 2\pi \times 2.5$  MHz and  $\omega_z = 2\pi \times 5$  MHz, the closest trap distance is  $d = 10$   $\mu$ m, the shuttling velocity is  $v = 0.2$  m/s and the laser addressing width is  $w = 10$   $\mu$ m. The two black dashed lines indicate the entry and exit times of the mobile ion within the operation region, corresponding to  $t_0 = -w/(2v)$  and  $T = w/v$ . (b) Heatmap showing the normalized oscillation amplitude in the  $x$ -direction,  $\xi_{x,\max}/d$ , as a function of the frequency ratios  $f_1/f_3$  and  $f_2/f_3$ . The contours indicate specific values of  $\xi_{x,\max}/d$ . (c) Maximum displacement of the equilibrium positions of the ions, normalized as  $q_{\max}^{(0)}/d$ , plotted as a function of  $f_2/f_3$ .

operators (see Method),

$$\hat{\theta}(t) = -\frac{1}{2}f(t) \sum_{j,l,n=1}^2 u_n(t) b_j^n b_l^n \hat{\sigma}_j^z \hat{\sigma}_l^z. \quad (6)$$

As a result, the full evolution operator associated with  $\hat{H}(t)$  can be factorized as

$$\hat{U}(t) = \hat{U}_D^\dagger(t) \mathcal{T} \exp \left[ -\frac{i}{\hbar} \int_{t_0}^t \hat{\theta}(\tau) d\tau \right] \hat{U}_0(t), \quad (7)$$

where  $\hat{U}_0(t) = \mathcal{T} \exp \left[ -\frac{i}{\hbar} \int_{t_0}^t \hat{H}_0(\tau) d\tau \right]$  is the free evolution operator in the absence of laser driving.

We define  $\hat{M}(t)$  as the operation on top of the free evolution, which can be represented as

$$\hat{M}(t) = \exp \left\{ -\frac{i}{\hbar} \sum_{j,n=1}^2 \left[ m\dot{u}_n(t)\hat{Z}_n - u_n(t)\hat{P}_n \right] b_j^n \hat{\sigma}_j^z \right\} \exp \left[ \frac{i}{2\hbar} \int_{t_0}^t d\tau f(\tau) \sum_{j,l,n=1, j \neq l}^2 u_n(\tau) b_j^n b_l^n \hat{\sigma}_j^z \hat{\sigma}_l^z \right] \quad (8)$$

where we have ignored irrelevant phases. To ensure at  $t = t_0 + T$  that  $\hat{M}$  is a gate operator of the controlled-phase-flip (CPF) gate, we require that

$$u_n(t_0 + T) = 0, \quad (9)$$

$$\dot{u}_n(t_0 + T) = 0, \quad (10)$$

and

$$\phi(t_0 + T) = \frac{1}{2\hbar} \int_{t_0}^{t_0 + T} d\tau f(\tau) \sum_{j,l,n=1, j \neq l}^2 u_n(\tau) b_j^n b_l^n = -\frac{\pi}{4}. \quad (11)$$

**Constraints.** The derivation above relies on operating in a regime where the dynamical normal-mode description remains valid during transport. We now examine the corresponding constraints on the system parameters. In our model, we assume that each ion is initially at its equilibrium position within its local trap, so there is no intrinsic oscillation due to the trapping potential. As the moving ion approaches and interacts with the stationary ion via Coulomb forces, the equilibrium positions of the two ions are displaced equally but in opposite directions from their respective trap centers. Additionally, the Coulomb interaction induces anti-symmetric oscillations of the ions around their new, shifted equilibrium positions, with both ions oscillating with equal amplitude but in opposite directions.

The DTG scheme requires an adiabatic shuttling such that  $|\xi_i(t)| \ll R(t)$ , which imposes constraints on the choice of parameters  $v$ ,  $d$  and  $\omega_{x,y}$ . This condition can be reformulated as  $\xi_{\mu,\max}/d \ll 1$ , where  $\xi_{\mu,\max}$  represents the maximum oscillation amplitude during the gate operation in the  $\mu$ -direction. We identify three frequency scales that influence  $\xi_{\mu,\max}/d$ . The first is  $f_1 = v/d$ , which characterizes the dynamics of the shuttling process. The second is  $f_2 = \sqrt{\frac{e^2}{4\pi\epsilon_0 m d^3}}$ , associated with the strength of the Coulomb interaction between the two ions. The third is  $f_3 = \omega_{x,y}$ , reflecting the strength of the trapping potential. Fig. 2b illustrates the normalized oscillation amplitude  $\xi_{\mu,\max}/d$  as a function of the frequency ratios  $f_1/f_3$  and  $f_2/f_3$ . For simplicity, only  $\xi_{x,\max}$  is plotted, as  $\xi_{x,\max}$  and  $\xi_{y,\max}$  are of comparable magnitude. In the strong trapping regime, where  $f_1/f_3 \ll 1$  or  $f_2/f_3 \ll 1$ , the confinement provided by the trap effectively suppresses the ion's oscillatory motion, ensuring that  $\xi_{\mu,\max}/d \ll 1$ , satisfying the adiabatic shuttling requirement. Conversely, when  $f_1 \sim f_2 \sim f_3$ , the oscillations become more pronounced.

We further examine the displacement of the equilibrium positions of the ions caused by the Coulomb interaction. Fig. 2c shows the normalized displacement  $q_{\max}^{(0)}/d$  as a function of  $f_2/f_3$ , where  $q_{\max}^{(0)}$  represents

the maximum displacement during the gate operation. While it is theoretically possible for a DTG to operate effectively even with large displacements, we opt to perform operations in the small-displacement regime, where  $q_{\max}^{(0)}/d \ll 1$ . Operating in this regime offers several advantages. First, during gate operation, laser beams are used to drive the interaction, and the laser intensity is typically strongest and most robust at the beam center. By minimizing the displacement, the ions remain closer to the center of the laser field, thereby reducing the required laser power and undesired fluctuation. Second, a smaller displacement ensures greater stability within the trap. Displacement from the trap minimum introduces greater micromotion for the ions, which can degrade the fidelity of the gate operation. By confining the ions to a small-displacement regime, we enhance the robustness of the gate while optimizing the power efficiency of the system.

**Pulse shaping.** In an ideal geometric-phase gate, one would satisfy the closure conditions  $u_n(t_0 + T) = 0$  and  $\dot{u}_n(t_0 + T) = 0$  for all motional modes while accumulating the target entangling phase  $\phi(t_0 + T) = -\pi/4$ . In practice, the time-dependent mode frequencies  $\Omega_n(t)$  and the finite parametrization of the drive prevent these constraints from being met exactly. We therefore quantify the residual spin-motion entanglement by the final phase-space displacement,  $\Delta u_n = u_n(t_0 + T)$ ,  $\Delta \dot{u}_n = \dot{u}_n(t_0 + T)$  and the phase mismatch  $\Delta\phi = \phi(t_0 + T) + \pi/4$ . To leading order in these residuals, the gate fidelity can be expressed as

$$F = 1 - \frac{m}{2\hbar} \sum_{n=1}^2 \left( \frac{|\Delta \dot{u}_n|^2}{\omega_z} + \omega_z |\Delta u_n|^2 \right) (2\bar{N}_n + 1) - |\Delta\phi|^2, \quad (12)$$

where  $\bar{N}_n$  is the mean phonon occupation of mode  $n$  in the initial thermal state.

We optimize the gate performance by tailoring the amplitude envelope  $\chi(t)$  and the detuning  $\mu$  of the driving field [27]. The drive is applied only while the moving ion traverses the operation region, so that  $\chi(t) = 0$  outside the gate window,  $[t_0, t_0 + T]$ , with  $t_0 = -w/(2v)$  and  $T = w/v$ . Within this interval, we parametrize  $\chi(t)$  as a piecewise-constant function consisting of five equal-duration segments. The set of segment amplitudes  $\{\chi_k(t)\}$  and the detuning  $\mu$  are then determined by numerical optimization to maximize  $F$  for a given experimental configuration.

Fig. 3 shows two representative optimized solutions for a pair of  $^{171}\text{Yb}^+$  ions with  $d = w = 10 \mu\text{m}$ . For a shuttling velocity  $v = 0.2 \text{ m/s}$ , the optimal parameters are  $\mu = -0.06\omega_z$ , and the corresponding five-segment envelope is shown in Fig. 3a; the resulting phase-space tra-

jectories of both dynamical modes return to the origin with high accuracy (Fig. 3b). For a faster transport,  $v = 0.5$  m/s, the optimal detuning shifts to  $\mu = -0.02\omega_z$  with a modified envelope (Fig. 3c), again yielding near-closed trajectories (Fig. 3d). In both cases, the optimized five-segment drive achieves an intrinsic fidelity approaching  $F \approx 1 - 10^{-7}$  assuming initial thermal states at the Doppler limit.

**Error analysis.** The intrinsic error of the drive-through gate arises from residual spin-motion entanglement due to imperfect closure of the phase-space trajectories. With optimized pulse shaping, this contribution can be suppressed to the level of  $\delta F_1 \sim 10^{-7}$ , indicating that the protocol-level error is negligible under idealized conditions.

A second class of errors is associated with the shuttling-induced motion of the ions in the  $x$ - $y$  plane. Such motion leads to fluctuations in the effective Rabi frequency experienced by the ions during the interaction. For small oscillations in the  $x$ - $y$  plane, the resulting infidelity scales as  $\delta F_2 \approx (\pi/2) (\xi_{\mu,\max}/w)^4$  [28], which remains below  $10^{-10}$  within the parameter regime considered. This contribution is therefore strongly suppressed by operating in the small-displacement regime identified above.

Additional errors originate from standard experimental imperfections common to trapped-ion platforms. In particular, higher-order terms beyond the Lamb–Dicke approximation for thermal motion along the  $z$  axis contribute an estimated infidelity of order  $\delta F_3 \approx 10^{-4}$  for ions pre-cooled to the Doppler temperature [29]. Other effects, including crosstalk and laser intensity drift, can be further suppressed using established pulse-shaping and compensation techniques [30]. The unwanted Stark shift associated with the  $\sigma_z \otimes \sigma_z$  interaction can be eliminated by echo pulses [31, 32]. Although optical phase noise is not treated explicitly, its effect can be mitigated using established optimized control protocols [33].

**Scalable architecture.** Having established the feasibility and error characteristics of the drive-through gate at the two-ion level, we now discuss how this primitive can be incorporated into scalable trapped-ion architectures. The key feature of the DTG scheme is that entanglement is generated during continuous transport, allowing moving ions to function as communication qubits that interact sequentially with spatially separated stationary ions acting as memory units. As an illustrative example, Fig. 4a shows how a distributed  $N$ -qubit GHZ state  $(|0\rangle^{\otimes N} + |1\rangle^{\otimes N})/\sqrt{2}$  can be generated using a single moving ion and  $N$  stationary ions. The moving ion (Ion  $X$ ) is first prepared in a superposition state and subsequently undergoes a sequence of drive-through CNOT interactions with stationary ions 1 through  $N - 1$ . A final drive-through SWAP operation with stationary ion  $N$  transfers the entanglement to the stationary register, resulting in a GHZ state distributed across the memory

ions. This example highlights how a single mobile qubit can mediate long-range entanglement without requiring repeated stopping, merging, or reconfiguration steps.

Beyond this illustrative protocol, the drive-through gate naturally supports modular architectures in which stationary ion arrays serve as local memory units while moving ions provide inter-module connectivity. Figures 4b and 4c depict two representative realizations of this concept. In the linear architecture shown in Fig. 4b, a moving ion is initialized in a designated cooling and preparation region, interacts sequentially with multiple memory arrays via drive-through gates, and can be recycled after completing its interactions. Fig. 4c illustrates a race-track architecture in which multiple moving ions circulate along closed paths, periodically passing through cooling and initialization zones. Such architectures enable continuous operation and flexible routing of quantum information while avoiding the transport overhead associated with repeated stopping and re-cooling.

Importantly, the present work focuses on establishing the gate-level physical mechanism underlying the drive-through paradigm. The system-level compilation and architectural implications of this approach have been explored separately, where the continuous-transport model is shown to be compatible with efficient circuit execution and resource management [34]. Together, these results indicate that the DTG scheme provides a viable building block for scalable, modular trapped-ion quantum computing architectures.

## Discussion

The DTG scheme builds upon the advantages of the QCQD architecture while addressing some of its key drawbacks, making it a promising alternative for scalable trapped-ion quantum computing. Similar to the QCQD approach, the DTG scheme organizes ions into multiple arrays, referred to as modules, and moves the communication ion close to a specific module during entanglement operations. This design avoids the need for scaling laser power with increasing inter-ion separation during entanglement, maintaining efficiency even in large-scale systems. However, unlike the QCQD architecture, the DTG scheme eliminates the need for the communication qubit to stop for entanglement with stationary ions. This continuous motion avoids motional heating caused by the non-uniform acceleration and deceleration of ions, which is a significant challenge in QCQD systems. Moreover, in the DTG framework, the communication ions can be pre-cooled prior to the entanglement operation, eliminating the need for employing different ion species for sympathetic cooling during ion shuttling and thereby reducing system complexity and resource overhead. The DTG scheme also offers flexibility for distributed quantum operations, including superdense coding, quantum teleportation, and the generation of multipartite entanglement. By avoiding the severe motional heating associated with splitting and merging processes in QCQD

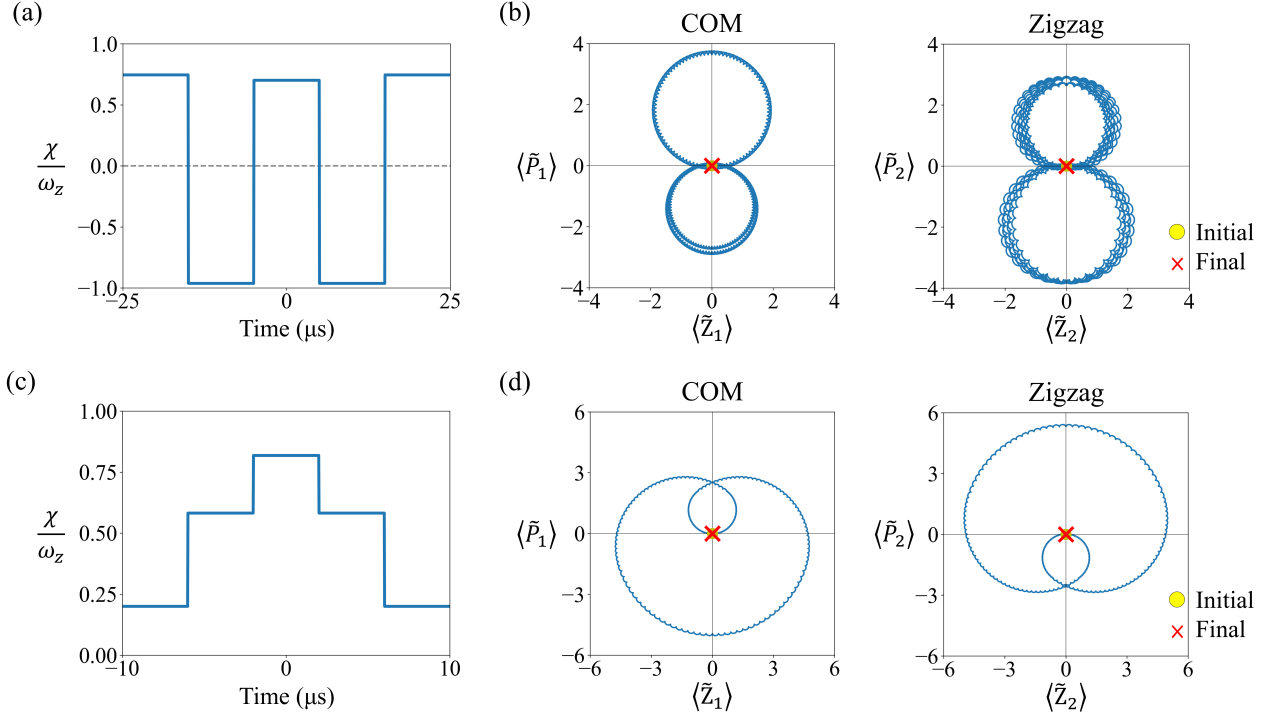


Figure 3. **Optimized pulse shape and phase space trajectory.** (a) Optimized pulse shape and (b) phase space trajectories with  $v = 0.2 \text{ m/s}$  and  $\mu = -0.06\omega_z$ . (c) Optimized pulse shape and (d) phase space trajectories with  $v = 0.5 \text{ m/s}$  and  $\mu = -0.02\omega_z$ . In both cases,  $d = 10 \text{ } \mu\text{m}$ ,  $w = 10 \text{ } \mu\text{m}$ ,  $\omega_{x,y} = 2\pi \times 2.5 \text{ MHz}$  and  $\omega_z = 2\pi \times 5 \text{ MHz}$ .  $\langle \tilde{Z}_n \rangle$  and  $\langle \tilde{P}_n \rangle$  denote the normalized expectation values of the position and momentum operators in the interaction picture for the center-of-mass ( $n = 1$ ) and zigzag ( $n = 2$ ) modes. In (b) and (d), the yellow circle (initial) and red cross (final) indicate the phase-space displacements.

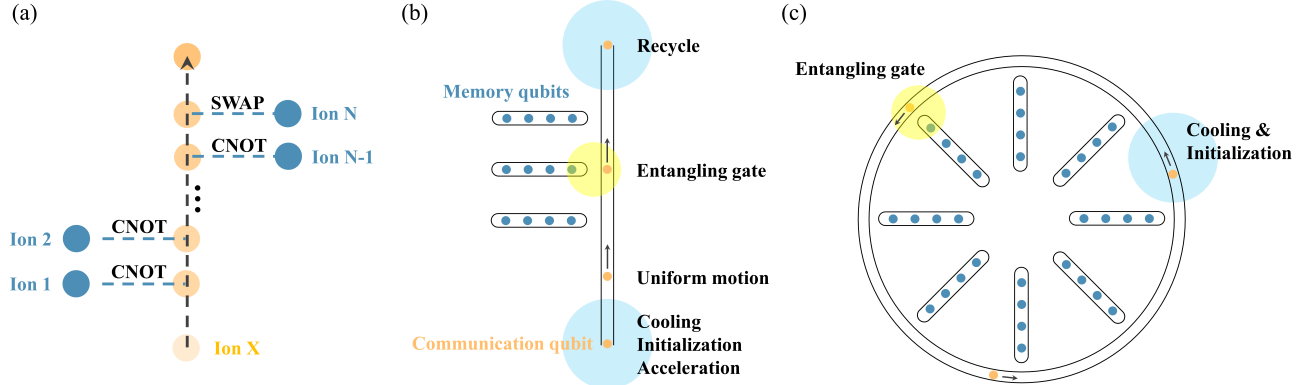


Figure 4. **Scalable architecture.** (a) Schematic for generating a distributed  $N$ -qubit GHZ state using a single moving ion and  $N$  stationary ions. The moving ion (Ion X) is initialized to a superposition state and sequentially interacts with stationary ions 1 through  $N - 1$  via drive-through CNOT gates. A final drive-through SWAP gate with stationary ion  $N$  completes the process, creating a GHZ state distributed among the  $N$  stationary ions. (b) Linear architecture with static ion arrays serving as memory units. A single moving ion is initialized in the cooling and initialization zone, interacts with the memory ions via drive-through gates, and can be recycled afterward. (c) Race-track architecture where multiple moving ions travel along a closed track, interacting with memory ions via drive-through gates. The moving ions can be re-cooled and re-initialized after completing a cycle.

systems, the DTG scheme enables a more efficient and reliable method for connecting distant ion modules. This capability provides a pathway toward scalable modular trapped-ion architectures.

In conclusion, we theoretically demonstrate and analyze a drive-through entangling gate between a stationary ion and a mobile ion that remains in continuous motion during the interaction. Our scheme simplifies the transport protocol in existing QCCD architectures and is feasible with current quantum technology. Precise control over ion positioning has been demonstrated for transport gates [22], and the Raman laser scheme for the adiabatic  $\sigma_z \otimes \sigma_z$  gate has been well established for decades. By combining these techniques, our approach provides a practical route for realizing entangling gates in trapped-ion systems based on continuous ion transport.

Future work could further refine this scheme to reduce residual errors and explore its integration into larger modular trapped-ion architectures.

## Method

**Derivation of the transformed Hamiltonian.** We deal with a Hamiltonian  $\hat{H}(t) = \hat{H}_0(t) + \hat{H}_1(t)$  with

$$\begin{aligned}\hat{H}_0(t) &= \frac{1}{2} [\hat{p}^2 + \omega^2(t) \hat{q}^2], \\ \hat{H}_1(t) &= f(t) \hat{q},\end{aligned}$$

which is a simplified version but the result can be generalized to incorporate the state-dependence as in the main text. Here,  $\hat{q}$  and  $\hat{p}$  are the position and momentum operators,  $\omega(t)$  is the time-dependent frequency, and  $f(t)$  is the driving force. Note that we have set mass  $m = 1$  for simplicity. Define the unitary transformation

$$\hat{U}_D = \exp \left\{ \frac{i}{\hbar} [\dot{u}(t) \hat{q} - u(t) \hat{p}] \right\}$$

where  $u(t)$  satisfies the classical equation of motion of the oscillator

$$\ddot{u}(t) + \omega^2(t)u(t) = f(t).$$

In this sense,  $\hat{U}_D$  is a displacement operator whose displacement follows the classical trajectory of the system. The unitary transformation  $\hat{U}_D$  transforms  $\hat{H}(t)$  into

$$\tilde{H}(t) = \hat{U}_D \hat{H}(t) \hat{U}_D^\dagger - i\hbar \hat{U}_D \frac{\partial \hat{U}_D^\dagger}{\partial t}.$$

The first term is given by

$$\begin{aligned}\hat{U}_D \hat{H}(t) \hat{U}_D^\dagger &= \frac{1}{2} \left\{ [\hat{p} - \dot{u}(t)]^2 + \omega^2(t) [\hat{q} - u(t)]^2 \right\} + f(t) [\hat{q} - u(t)] \\ &= \frac{1}{2} [\hat{p}^2 + \omega^2(t) \hat{q}^2] - \dot{u}(t) \hat{p} + \frac{1}{2} \dot{u}^2(t) - \omega^2(t) u(t) \hat{q} \\ &\quad + \frac{1}{2} \omega^2(t) u^2(t) + f(t) \hat{q} - f(t) u(t).\end{aligned}$$

The time derivative of  $\hat{U}_D^\dagger$  is

$$\begin{aligned}\frac{\partial \hat{U}_D^\dagger}{\partial t} &= \frac{i}{\hbar} \exp \left[ \frac{i}{2\hbar} u(t) \dot{u}(t) \right] \exp \left[ \frac{i}{\hbar} u(t) \hat{p} \right] \\ &\quad \times \left[ \frac{1}{2} \dot{u}^2(t) + \frac{1}{2} u(t) \ddot{u}(t) + \dot{u}(t) \hat{p} - \ddot{u}(t) \hat{q} \right] \\ &\quad \times \exp \left[ -\frac{i}{\hbar} \dot{u}(t) \hat{q} \right].\end{aligned}$$

Thus, the second term is

$$\begin{aligned}-i\hbar \hat{U}_D \frac{\partial \hat{U}_D^\dagger}{\partial t} &= \exp \left[ \frac{i}{\hbar} \dot{u}(t) \hat{q} \right] \left[ \frac{1}{2} \dot{u}^2(t) + \frac{1}{2} u(t) \ddot{u}(t) + \dot{u}(t) \hat{p} - \ddot{u}(t) \hat{q} \right] \\ &\quad \times \exp \left[ -\frac{i}{\hbar} \dot{u}(t) \hat{q} \right] \\ &= -\frac{1}{2} \dot{u}^2(t) + \frac{1}{2} u(t) [-\omega^2(t)u(t) + f(t)] + \dot{u}(t) \hat{p} - \ddot{u}(t) \hat{q}.\end{aligned}$$

Combining the two terms, we have

$$\begin{aligned}\tilde{H}(t) &= \frac{1}{2} [\hat{p}^2 + \omega^2(t) \hat{q}^2] + [-\ddot{u}(t) - \omega^2(t)u(t) + f(t)] \hat{q} \\ &\quad + \left[ -\frac{1}{2} f(t) u(t) \right] \\ &= \frac{1}{2} [\hat{p}^2 + \omega^2(t) \hat{q}^2] - \frac{1}{2} f(t) u(t) \\ &= \hat{H}_0(t) + \hat{\theta}(t),\end{aligned}$$

where  $\hat{\theta}(t) = -\frac{1}{2} f(t) u(t)$  is the geometric phase term. This derivation can be generalized by allowing  $f(t)$  and  $u(t)$  to incorporate state-dependent operators. Under this extension, the geometric phase term  $\hat{\theta}(t)$  yields the  $\sigma_z \otimes \sigma_z$  interaction described in the main text.

---

[1] Blatt, R. & Wineland, D. Entangled states of trapped atomic ions. *Nature* **453**, 1008–1015 (2008).

[2] Monroe, C. & Kim, J. Scaling the ion trap quantum processor. *Science* **339**, 1164–1169 (2013).

[3] Harty, T. *et al.* High-fidelity preparation, gates, memory, and readout of a trapped-ion quantum bit. *Physical Review Letters* **113**, 220501 (2014).

[4] Ballance, C., Harty, T., Linke, N., Sepiol, M. & Lucas, D. High-fidelity quantum logic gates using trapped-ion hyperfine qubits. *Physical Review Letters* **117**, 060504 (2016).

[5] Gaebler, J. *et al.* High-fidelity universal gate set for  ${}^9\text{Be}^+$  ion qubits. *Physical Review Letters* **117**, 060505 (2016).

[6] Srinivas, R. *et al.* High-fidelity laser-free universal control of trapped ion qubits. *Nature* **597**, 209–213 (2021).

[7] Wright, K. *et al.* Benchmarking an 11-qubit quantum computer. *Nature Communications* **10** (2019).

[8] Wu, Y.-K. & Duan, L.-M. A two-dimensional architecture for fast large-scale trapped-ion quantum computing. *Chinese Physics Letters* **37**, 070302 (2020).

[9] Mehdi, Z., Ratcliffe, A. K. & Hope, J. J. Fast entangling gates in long ion chains. *Physical Review Research* **3**, 013026 (2021).

[10] Zhang, J. *et al.* Observation of a many-body dynamical phase transition with a 53-qubit quantum simulator. *Nature* **551**, 601–604 (2017).

[11] Leung, P. H. & Brown, K. R. Entangling an arbitrary pair of qubits in a long ion crystal. *Physical Review A* **98**, 032318 (2018).

[12] Murali, P., Debroy, D. M., Brown, K. R. & Martonosi, M. Architecting noisy intermediate-scale trapped ion quantum computers. In *2020 ACM/IEEE 47th Annual International Symposium on Computer Architecture (ISCA)*, 529–542 (IEEE, 2020).

[13] Monroe, C. *et al.* Large-scale modular quantum-computer architecture with atomic memory and photonic interconnects. *Physical Review A* **89**, 022317 (2014).

[14] Stephenson, L. *et al.* High-rate, high-fidelity entanglement of qubits across an elementary quantum network. *Physical Review Letters* **124**, 110501 (2020).

[15] Krutyanskiy, V. *et al.* Entanglement of trapped-ion qubits separated by 230 meters. *Physical Review Letters* **130**, 050803 (2023).

[16] Kielinski, D., Monroe, C. & Wineland, D. J. Architecture for a large-scale ion-trap quantum computer. *Nature* **417**, 709–711 (2002).

[17] Wan, Y. *et al.* Ion transport and reordering in a 2D trap array. *Advanced Quantum Technologies* **3** (2020).

[18] Bruzewicz, C. D., Chiaverini, J., McConnell, R. & Sage, J. M. Trapped-ion quantum computing: Progress and challenges. *Applied Physics Reviews* **6** (2019).

[19] Pino, J. M. *et al.* Demonstration of the trapped-ion quantum CCD computer architecture. *Nature* **592**, 209–213 (2021).

[20] Moses, S. *et al.* A race-track trapped-ion quantum processor. *Physical Review X* **13**, 041052 (2023).

[21] Saki, A. A., Topaloglu, R. O. & Ghosh, S. Muzzle the shuttle: Efficient compilation for multi-trap trapped-ion quantum computers. In *2022 Design, Automation & Test in Europe Conference & Exhibition (DATE)*, 322–327 (IEEE, 2022).

[22] Tinkey, H. N., Clark, C. R., Sawyer, B. C. & Brown, K. R. Transport-enabled entangling gate for trapped ions. *Physical Review Letters* **128**, 050502 (2022).

[23] Leibfried, D., Knill, E., Ospelkaus, C. & Wineland, D. J. Transport quantum logic gates for trapped ions. *Physical Review A* **76**, 032324 (2007).

[24] Lizuain, I., Palmero, M. & Muga, J. G. Dynamical normal modes for time-dependent hamiltonians in two dimensions. *Physical Review A* **95**, 022130 (2017).

[25] García-Ripoll, J. J., Zoller, P. & Cirac, J. I. Coherent control of trapped ions using off-resonant lasers. *Physical Review A* **71**, 062309 (2005).

[26] Zhu, S.-L., Monroe, C. & Duan, L.-M. Arbitrary-speed quantum gates within large ion crystals through minimum control of laser beams. *Europhysics Letters (EPL)* **73**, 485–491 (2006).

[27] Choi, T. *et al.* Optimal quantum control of multimode couplings between trapped ion qubits for scalable entanglement. *Physical Review Letters* **112**, 190502 (2014).

[28] Lin, G.-D. *et al.* Large-scale quantum computation in an anharmonic linear ion trap. *EPL (Europhysics Letters)* **86**, 60004 (2009).

[29] Sørensen, A. & Mølmer, K. Entanglement and quantum computation with ions in thermal motion. *Physical Review A* **62**, 022311 (2000).

[30] Blümel, R., Grzesiak, N., Pisenti, N., Wright, K. & Nam, Y. Power-optimal, stabilized entangling gate between trapped-ion qubits. *npj Quantum Information* **7** (2021).

[31] Clark, C. R. *et al.* High-fidelity bell-state preparation with  ${}^{40}\text{Ca}^+$  optical qubits. *Physical Review Letters* **127**, 130505 (2021).

[32] Sawyer, B. C. & Brown, K. R. Wavelength-insensitive, multispecies entangling gate for group-2 atomic ions. *Physical Review A* **103**, 022427 (2021).

[33] Steane, A. M., Imreh, G., Home, J. P. & Leibfried, D. Pulsed force sequences for fast phase-insensitive quantum gates in trapped ions. *New Journal of Physics* **16**, 053049 (2014).

[34] Chang, C.-M., Jiang, J.-H. R., Chiou, D.-W., Hsu, T. & Lin, G.-D. Quantum circuit compilation for trapped-ion processors with the drive-through architecture. *IEEE Transactions on Quantum Engineering* **6**, 1–14 (2025).